Journal of Alloys and Compounds 509 (2011) 3627–3631

Contents lists available at ScienceDirect

Journal of Alloys and Compounds

journal homepage: www.elsevier.com/locate/jallcom

Corrosion behavior of magnetic refrigeration material La–Fe–Co–Si in distilled water

Min Zhang*, Yi Long, Rong-chang Ye, Yong-qin Chang

School of Materials Science and Engineering, University of Science and Technology Beijing, 30 XueYuan Road, Haidian District, Beijing 100083, PR China

ARTICLE INFO

Article history:
Received 25 August 2009
Received in revised form
15 December 2010
Accepted 17 December 2010
Available online 23 December 2010

Keywords:
Magnetic refrigeration material
Electrochemical preferential corrosion
$La(Fe_{0.94}Co_{0.06})_{11.7}Si_{1.3}$

ABSTRACT

The corrosion behavior of magnetic refrigeration material $La(Fe_{0.94}Co_{0.06})_{11.7}Si_{1.3}$ in distilled water has been studied using X-ray diffraction analysis, weight loss method, scanning electron microscopy and X-ray photoelectron spectroscopy. Results show that $La(Fe_{0.94}Co_{0.06})_{11.7}Si_{1.3}$ compound suffers electrochemical preferential corrosion in distilled water. $La(Fe_{0.94}Co_{0.06})_{11.7}Si_{1.3}$ compound contains three phases which are matrix phase, a small amount of α-Fe phase and La-rich phase. The matrix phase with $NaZn_{13}$ structure works as anode to be corroded. The final corrosion products on sample surface are La_2O_3, γ-Fe(OOH), $Co(OH)_2$ and H_2SiO_3, respectively. Corrosion has decreased the maximum magnetic entropy change of the compound.

© 2010 Elsevier B.V. All rights reserved.

1. Introduction

$La(Fe_xSi_{1-x})_{13}$ compounds with cubic $NaZn_{13}$-type structure have been considered as new refrigerant for magnetic refrigeration near room temperature since the discovery of their giant magnetocaloric effect associated with low cost of raw material [1–4]. However, low Curie temperature and hysteresis loss restrain their application. Recent investigations reveal that partial substitution of Fe by Co in $La(Fe_xSi_{1-x})_{13}$ compounds leads to increase in Curie temperature and the weakening of the first-order magnetic transition. Although the substitution of Co produces a decrease in magnetic entropy change, a small hysteresis loss and a large RCP can be realized [5–11]. Besides the reduction of hysteresis loss, preparation time for $La(Fe,Co,Si)_{13}$ compounds is shortened through new methods [12,13].

On the other hand, heat exchange between $La(Fe_xSi_{1-x})_{13}$ magnetic refrigerants and the load must be done through fluid media because in magnetic refrigerators, the $La(Fe_xSi_{1-x})_{13}$ compounds work in solid state. Most of the prototypes use water or water based fluids as heat exchange media [14,15]. However, the $La(Fe_xSi_{1-x})_{13}$ compounds will be corroded seriously in water without protection, thus directly influence the performance as well as the working life of magnetic refrigerator. Therefore, it is of great significance to study the corrosion behavior of $La(Fe_xSi_{1-x})_{13}$ materials. In this paper, corrosion behavior of La $(Fe_{0.94}Co_{0.06})_{11.7}Si_{1.3}$ magnetic refrigerant was studied.

2. Experimental

The $La(Fe_{0.94}Co_{0.06})_{11.7}Si_{1.3}$ samples were melted by intermediate frequency induction furnace with pure elements La, Fe, Co, and Si, and then cast into ingots in a water-cooling copper mold. The purities of La, Fe, Co, and Si were 99.9 wt%, 99.99 wt%, 99.9 wt% and 99.999 wt%, respectively. The ingots were annealed at (1323 ± 5) K in sealed quartz tube with high vacuum of 10^{-3} Pa for 1200 h and then quenched in ice water. Samples with dimensions of 10 mm × 10 mm × 3 mm were cut from the ingots and cold mounted in epoxy resin with only one surface outside. Samples for corrosion testing were mechanically wet polished up to 800 grit by water-proof SiC polishing paper, while those for scanning electron microscope (SEM) observation were mechanically wet polished up to 1200 grit by water-proof SiC polishing paper and then polished to mirror surface by polishing grease. Samples after polishing were cleaned in distilled water, alcohol and dried by hair drier in sequence. The exposed surface area was 1 cm^2. All the corrosion studies were carried out in distilled water.

The crystalline structure of $La(Fe_{0.94}Co_{0.06})_{11.7}Si_{1.3}$ compound was studied by X-ray diffraction (XRD) by Rigaku D/Max 12,000 diffractometer with Cu Kα ($\lambda = 1.5406 \times 10^{-10}$ m) target and the results were analyzed by Jade 5.0. Corrosion behavior of the compounds was investigated firstly by weight loss method. The corrosion rates were estimated from the weight loss after different immersion times. Then topography and composition on the surface of corroded samples were characterized by Cambridge S360 scanning electron microscope (SEM) equipped with X-ray energy-dispersive spectrometer (EDS). Chemical composition of corrosion products on the surface of samples was analyzed by X-ray photoelectron spectroscopy (XPS) with monochromatic Al Kα (1486.6 eV) target. Magnetic properties were measured by physical property measurement system (Versalab vibrating sample magnetometer, VSM).

3. Results and discussion

Fig. 1 shows the XRD pattern of $La(Fe_{0.94}Co_{0.06})_{11.7}Si_{1.3}$ compound after annealing for 1200 h. Most of the Bragg peaks belong to $NaZn_{13}$-type structure (1:13 phase, cubic with space group *Fm*3*c*, $a = 11.60$ Å), while a small amount of α-Fe phase and La-rich phase

* Corresponding author. Tel.: +86 1062334807; fax: +86 1062334807.
E-mail address: zhmn9459@gmail.com (M. Zhang).

0925-8388/$ – see front matter © 2010 Elsevier B.V. All rights reserved.
doi:10.1016/j.jallcom.2010.12.122

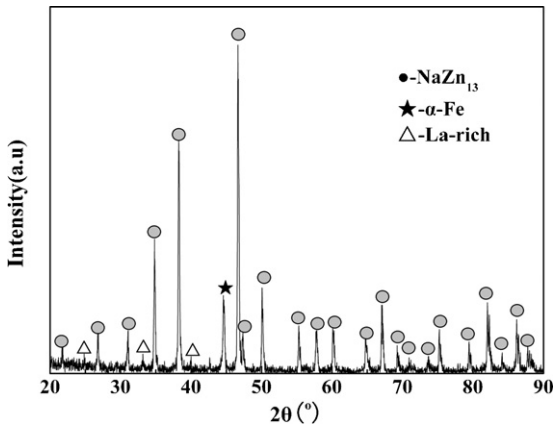

Fig. 1. X-ray diffraction pattern of $La(Fe_{0.94}Co_{0.06})_{11.7}Si_{1.3}$ compound.

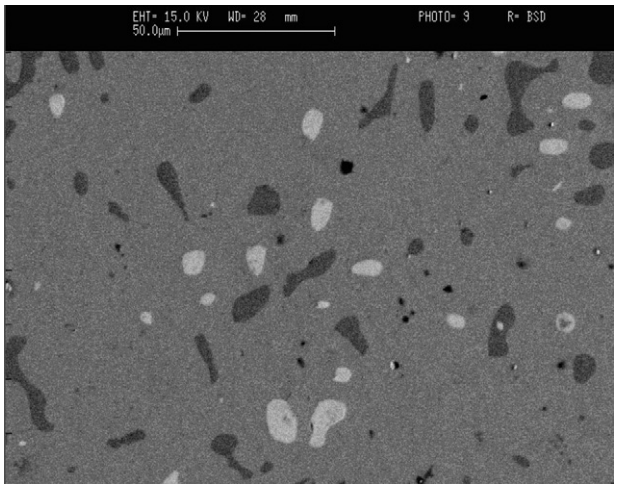

Fig. 2. SEM backscattered electron image of $La(Fe_{0.94}Co_{0.06})_{11.7}Si_{1.3}$ compound.

(tetragonal with space group *P*4/*nmm*, $a = 4.13$ Å, $c = 7.24$ Å) coexist. Furthermore, the sharpness of these Bragg peaks suggests a well-crystallized structure. The compound consists of three phases, which can be confirmed by the SEM backscattered electron image of sample (shown in Fig. 2). Three different colors stand for three different phases, namely, the gray phase, the black phase and the white phase. The gray phase is the matrix phase. Further examination was made by EDS analysis, shown in Table 1. According to XRD, SEM and EDS analysis, it can be seen that the matrix phase is 1:13 phase, the black phase is α-Fe phase and the white phase is La-rich phase.

In order to study the corrosion behavior of $La(Fe_{0.94}Co_{0.06})_{11.7}Si_{1.3}$ compound, the samples were immersed in distilled water for different times. Weight loss method was used to estimate corrosion rates according to the following equation:

$$\bar{V} = \frac{m_0 - m_1}{S \cdot t} \quad (1)$$

Table 1
Composition of phases.

Atom/%	La	Fe	Co	Si
Nominal composition	7.1	78.6	5.0	9.3
Gray phase	7.0	81.0	6.6	5.4
Black phase	0.9	93.0	4.8	1.2
White phase	32.7	24.4	11.1	31.8

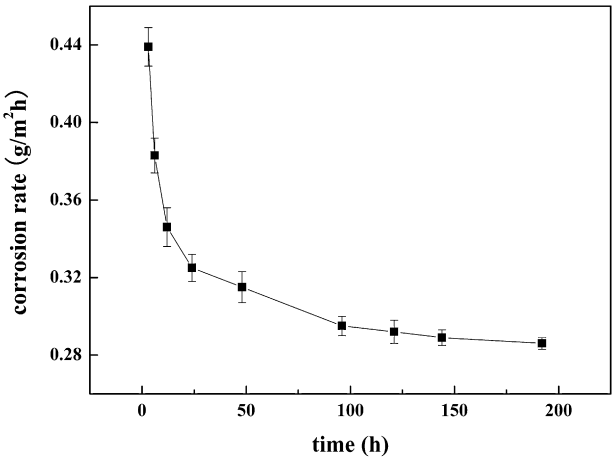

Fig. 3. Corrosion rate curve of $La(Fe_{0.94}Co_{0.06})_{11.7}Si_{1.3}$ compound in distilled water (temperature: 21 °C).

where m_0 and m_1 refer to weight before and after corrosion (wipe off the corrosion products) in gram, respectively, S is the exposed surface area in m^2 and t is the immersed time in hour. Fig. 3 shows the result of corrosion rate versus time of $La(Fe_{0.94}Co_{0.06})_{11.7}Si_{1.3}$ compound in distilled water. It can be seen that the corrosion rate of the material has a tendency to decrease with immersion time. The reasons are as follows: the corrosion process of $La(Fe_{0.94}Co_{0.06})_{11.7}Si_{1.3}$ compound in distilled water is an electrochemical process. At the beginning, sample surfaces are free and the corrosion resistance is very low, which leads to a high corrosion rate. As time goes on, the accumulation of corrosion products on sample surface increases, mass transportation of electrode reactions is blocked, so that the corrosion rate changes to a lower value. Since the products layer on sample surface is very loose, which could not form effective protection to the compound, corrosion would take place continuously unless protective measures are taken.

Fig. 4 shows the typical second electron image and backscattered electron image of the corroded surface of $La(Fe_{0.94}Co_{0.06})_{11.7}Si_{1.3}$ compound. Fig. 4(a) shows SEM image for the compound immerged in distilled water for 5 min. As shown in Fig. 4(a), corrosion occurs locally with corroded spots distributing randomly on sample surface. Shapes of these spots are almost circular as well as inner parts are pitted. Fig. 4(b) and (c) are the higher magnification second electron image and backscattered electron image of the same corroded spot in Fig. 4(a), respectively. It is found that the corroded phase is matrix phase and the left islands are α-Fe phase by EDS analysis. As time increasing, the amount of corroded spots increases, corrosion in original corroded spots becomes severity and corroded spots expand outwards along the surface. Some corroded spots in neighbor even connect to each other and thus form a larger corroded area. Fig. 4(d) shows second electron image for the sample immerged in distilled water for 15 min.

The results above indicate that the corrosion of $La(Fe_{0.94}Co_{0.06})_{11.7}Si_{1.3}$ in distilled water is caused by electrochemical inhomogeneity of compound surface. Due to the differences of electrode potential among phases, micro cells form easily between phases on sample surface when the sample is immerged in distilled water. SEM results show that corrosion occurs in the matrix mainly around α-Fe phase, which is different from NdFeB [16]. It suggests that the difference of electrode potential between matrix phase and α-Fe phase is bigger than that between La-rich phase and α-Fe phase. Thus electrochemical reaction occurs easier between matrix phase and α-Fe phase. During the corrosion process, α-Fe phase works as cathode, while matrix phase works as anode to be corroded. Corrosion occurs

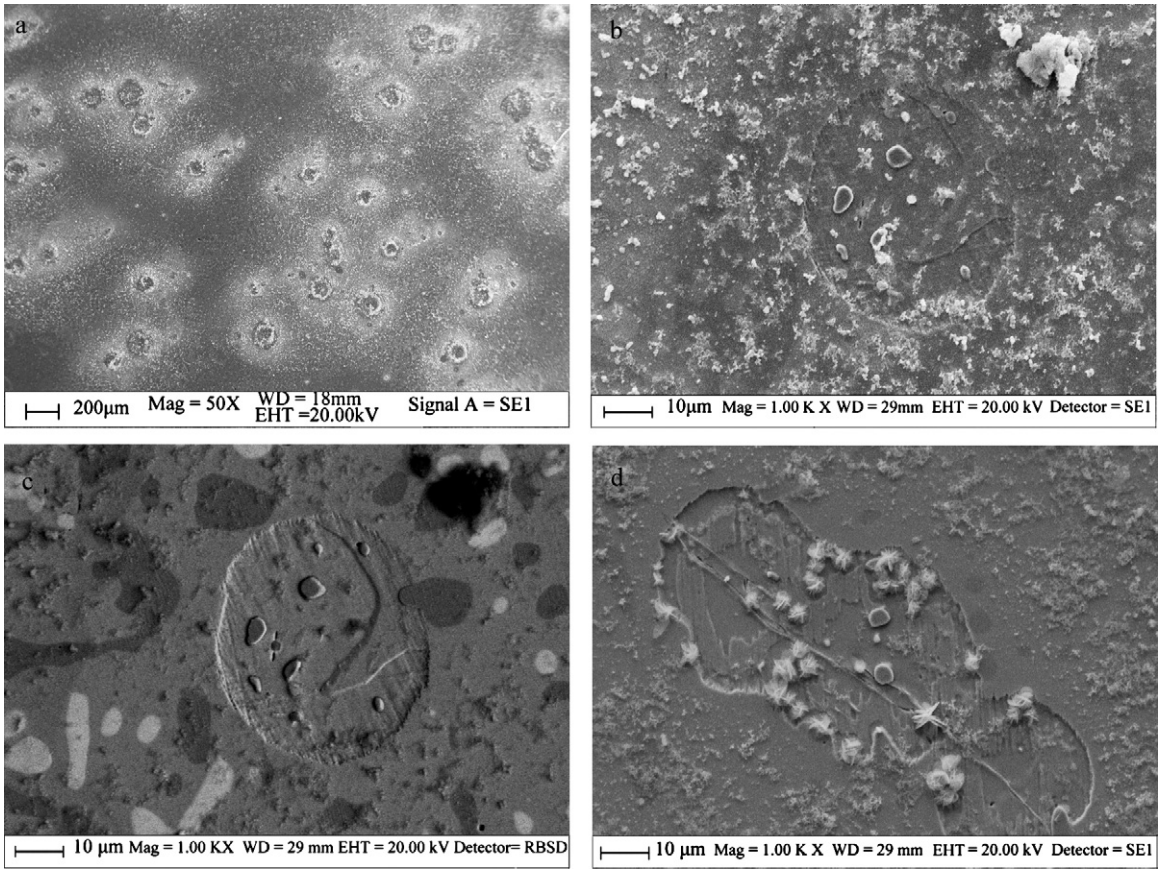

Fig. 4. SEM-micrographs of $La(Fe_{0.94}Co_{0.06})_{11.7}Si_{1.3}$ compound corroded in distilled water. (a) Second electron image of the corroded surface, (b) second electron image with higher magnification of local corrosion site, (c) backscattered electron image of the same local corrosion site in (b), and (d) second electron image of larger corrosion site

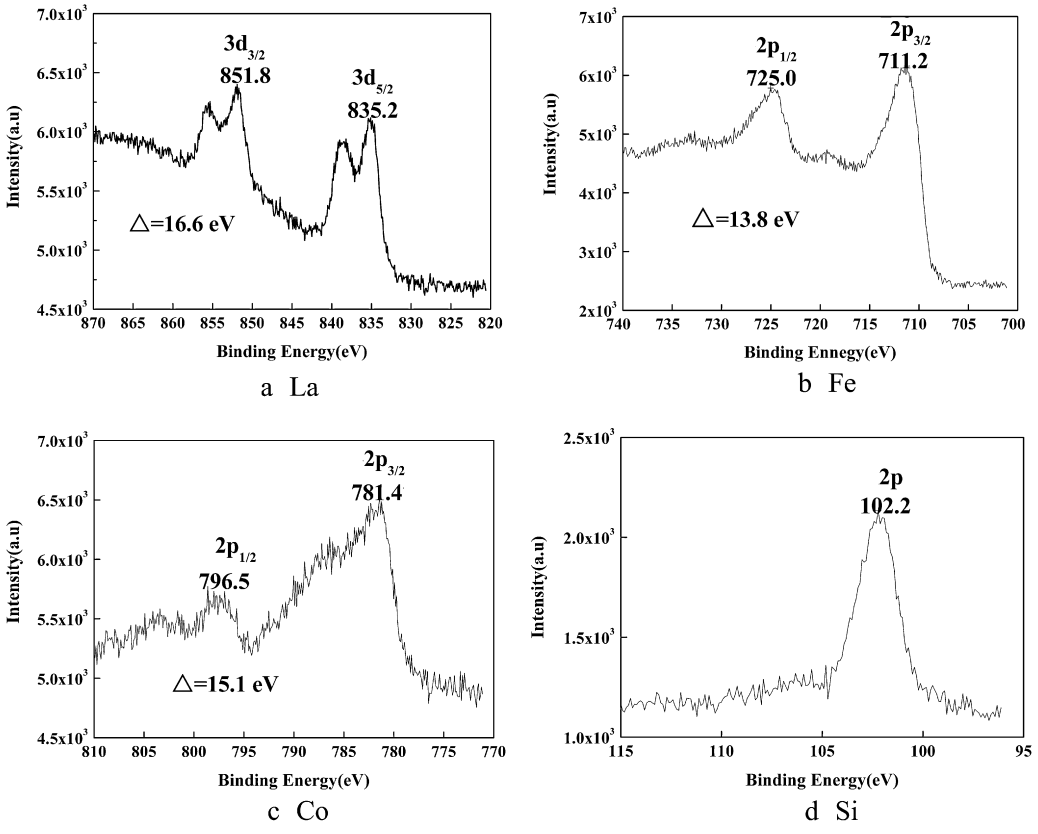

Fig. 5. XPS spectrums of the corrosion products. (a) La, (b) Fe, (c) Co, (d) Si.

Table 2
XPS analysis results of corrosion products.

Element	La	Fe	Co	Si
Bonding energy/eV	$3d_{5/2}$ 835.2 Δ = 16.6	$2p_{3/2}$ 711.2 Δ = 13.8	$2p_{3/2}$ 781.4 Δ = 15.1	2p 102.2
Chemical valence	+3	+3	+2	+4
Composition	La_2O_3	γ-Fe(OOH)	$Co(OH)_2$	H_2SiO_3

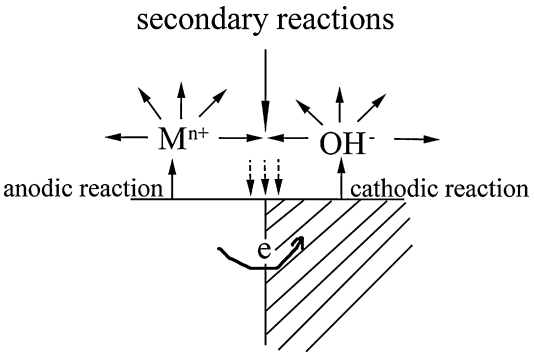

Fig. 6. Schematic diagram of electrochemical reactions.

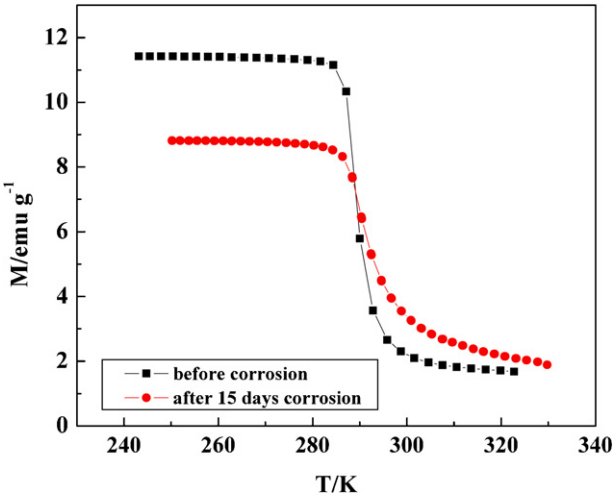

Fig. 8. Temperature dependent magnetization measured under an applied magnetic field 0.01 T for $La(Fe_{0.94}Co_{0.06})_{11.7}Si_{1.3}$ compounds before corrosion and after 15 days' corrosion.

in the matrix just adjacently to α-Fe phase in the beginning and extends outwards as time goes on.

The corrosion products on sample surface of $La(Fe_{0.94}Co_{0.06})_{11.7}Si_{1.3}$ compound were analyzed by X-ray photoelectron spectroscopy (XPS) analysis. Fig. 5 shows results of XPS spectrums of corrosion products after sample immerged in distilled water for one week. By referring to X-ray photoelectron spectrum handbook, chemical state of each element is identified and possible substance of each element is also suggested in Table 2. The symbol of Δ in Table 2 represents the binding energy space between La $3d_{5/2}$ and $3d_{3/2}$, Fe $2p_{3/2}$ and $2p_{1/2}$, Co $2p_{3/2}$ and $2p_{1/2}$, respectively. From Table 2 it is known that the final products of corrosion are La_2O_3, γ-Fe(OOH), $Co(OH)_2$ and H_2SiO_3, respectively. So for anodic reaction, the atoms of La, Fe, Co, Si in the matrix lose electrons and are oxidized into ions, with electrode reactions as follows:

$$La \rightarrow La^{3+} + 3e \quad (2)$$

$$Fe \rightarrow Fe^{2+} + 2e \quad (3)$$

$$Co \rightarrow Co^{2+} + 2e \quad (4)$$

$$Si + 3H_2O \rightarrow H_2SiO_3 + 4H^+ + 4e \quad (5)$$

For cathodic reaction, it might be hydrogen reduction or oxygen reduction. Further confirmation has been made by adding Na_2SO_3 into distilled water. Results indicate that corrosion is effectively suppressed due to the effect of oxygen elimination by Na_2SO_3. Thus cathodic reaction is as follows:

$$O_2 + 2H_2O + 4e \rightarrow 4OH^- \quad (6)$$

Schematic diagram of mass transportation process of corrosion is shown in Fig. 6. The ions produced by anodic reaction and cathodic reaction diffuse around. When they meet, secondary reactions occur as follows:

$$La^{3+} + 3OH^- \rightarrow La(OH)_3\downarrow \quad (7)$$

$$Fe^{2+} + 2OH^- \rightarrow Fe(OH)_2\downarrow \quad (8)$$

$$Co^{2+} + 2OH^- \rightarrow Co(OH)_2\downarrow \quad (9)$$

Due to its instability at presence of oxygen, $Fe(OH)_2$ turns into stable reddish-brown Fe(OOH) in the end and $La(OH)_3$ into La_2O_3 as well.

As time increasing, the accumulation of sediment on sample surface increases, which blocking mass transportation and increasing resistance of following corrosion reactions in these areas. Meanwhile, reduction of oxygen increases pH and decreases the corrosion in these regions, as shown in Fig. 7(a). Corrosion extends outwards along the surface and new corroded sports appear. As time goes on, corroded spots in neighbor grow bigger and connect to each other, as shown in Fig. 7(b). In the end, the matrix is corroded down with α-Fe phase and La-rich phase left out, as shown in Fig. 7(c).

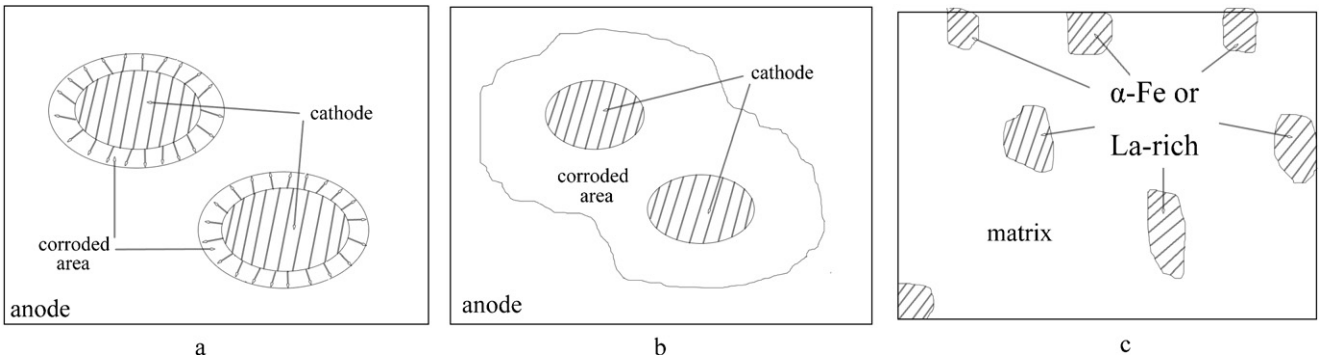

Fig. 7. Schematic graphs of corrosion mechanism.

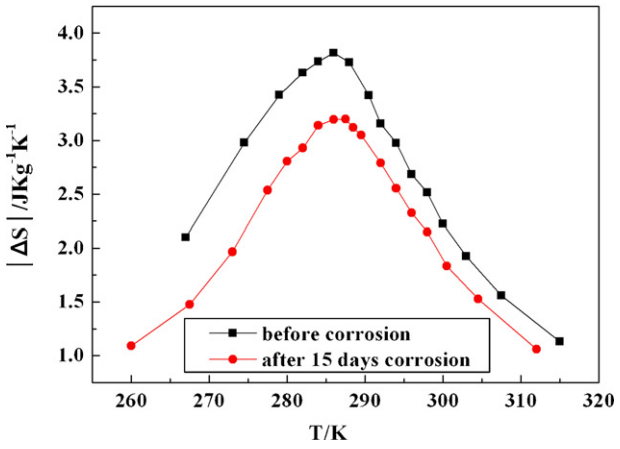

Fig. 9. Temperature dependent of the magnetic entropy change $|\Delta S|$ for $La(Fe_{0.94}C_{o0.06})_{11.7}Si_{1.3}$ compounds before corrosion and after 15 days' corrosion under a magnetic field change of 0–2 T.

In order to investigate the influence of corrosion on the magnetocaloric effect (MCE) of $La(Fe_{0.94}Co_{0.06})_{11.7}Si_{1.3}$ materials, magnetic properties were measured before and after corrosion. The thermomagnetic curves for $La(Fe_{0.94}Co_{0.06})_{11.7}Si_{1.3}$ compounds before and after 15 days' corrosion under an applied magnetic field 0.01 T are presented in Fig. 8. It shows that the Curie temperature T_C is increased slightly after 15 days' corrosion in distilled water. T_C before and after 15 days' corrosion are 290 K and 290.3 K, respectively. The magnetic entropy change $|\Delta S|$ is calculated from Maxwell relation using the collected magnetization data [17], as shown in Fig. 9. It can be seen that after 15 days' corrosion in distilled water the maximum entropy change $|\Delta S_{max}|$ decreased about 16%. The relative cooling power will decrease considerable proportion. For the $La(Fe_{0.94}Co_{0.06})_{11.7}Si_{1.3}$ compound, large magnetocaloric effect mainly comes from the matrix phase. Corrosion of the compound resulted in the reduction of matrix phase in the compound and then decreased $|\Delta S_{max}|$ as well.

4. Conclusions

The corrosion behavior of $La(Fe_{0.94}Co_{0.06})_{11.7}Si_{1.3}$ compound in distilled water has been studied. There are three phases, matrix phase with $NaZn_{13}$-type structure, a small amount of α-Fe phase and La-rich phase in $La(Fe_{0.94}Co_{0.06})_{11.7}Si_{1.3}$ compound after annealing at (1323 ± 5) K for 1200 h. The corrosion rate of the compound has a decreasing tendency with immersion time. The corrosion mechanism of $La(Fe_{0.94}Co_{0.06})_{11.7}Si_{1.3}$ is electrochemical preferential dissolution of the matrix phase, with oxygen reduction as the cathodic reaction. Corrosion is localized at matrix phase and expands mainly around the α-Fe phase. The final products of corrosion are La_2O_3, γ-Fe(OOH), $Co(OH)_2$ and H_2SiO_3 respectively. Corrosion has decreased the mass of matrix phase, resulted in the decrease of maximum magnetic entropy change of the compound.

Acknowledgements

This work was supported by The National High Technology Research and Development Program of China, The National Basic Research Program of China and the National Science Foundation of China.

References

[1] V.K. Pecharsky, K.A. Gschneidner Jr., Phys. Rev. Lett. 78 (1997) 4494.
[2] O. Tegus, E. Bru¨ck, K.H.J. Buschow, et al., Nature 415 (2002) 150.
[3] T. Liu, Y.G. Chen, Y.B. Tang, et al., J. Alloys Compd. 475 (2009) 672.
[4] M. Phejar, V. Paul-Boncour, L. Bessais, Intermetallics 18 (2010) 2301.
[5] J. Shen, Y.X. Li, J. Zhang, et al., J. Appl. Phys. 103 (2008) 07B317.
[6] A.T. Saito, T. Kobayashi, H. Tsuji, J. Magn. Magn. Mater. 310 (2007) 2808.
[7] Q.Y. Dong, H.W. Zhang, T.Y. Zhao, et al., Solid State Commun. 147 (2008) 266.
[8] J. Shen, Y.X. Li, F.X. Hu, et al., J. Appl. Phys. 105 (2009) 07A901.
[9] L. Jia, J.R. Sun, J. Shen, et al., J. Appl. Phys. 105 (2009) 07A924.
[10] B. Fu, Y. Long, P.J. Shi, et al., J. Rare Earths (Engl. Ed.) 28 (2010) 611.
[11] M. Jasinski, J. Liu, S. Jacobs, et al., J. Appl. Phys. 107 (2010) 09A953.
[12] J.L. Lyubina, O. Gutfleisch, M.D. Kuz'min, et al., J. Magn. Magn. Mater. 321 (2009) 3571.
[13] B.R. Hansen, L.T. Kuhn, C.R.H. Bahl, et al., J. Magn. Magn. Mater. 322 (2010) 3447.
[14] A. Fujita, S. Koiwai, S. Fujieda, et al., Jpn. J. Appl. Phys. 46 (2007) L154.
[15] N. Hirano, S. Nagaya, M. Takahashi, et al., J. Adv. Cryog. Eng. 47 (2002) 1027e1034.
[16] G.L. Yan, P.J. Mcguiness, J.P.G. Farr, et al., J. Alloys Compd. 478 (2009) 188.
[17] M. Balli, D. Fruchart, D. Gignoux, J. Appl. Phys. Lett. 92 (2008) 232505.